Constraint of glacial isostatic adjustment in the North Sea with geological relative sea level and GNSS vertical land motion data

Simon, K. M.; Riva, R. E.M.; Vermeersen, L. L.A.

DOI
10.1093/gji/ggab261

Publication date
2021

Document Version
Final published version

Published in
Geophysical Journal International

Geophysical Journal International

Geophys. J. Int. (2021) **227,** 1168–1180
Advance Access publication 2021 July 07
GJI Geodynamics and Tectonics

https://doi.org/10.1093/gji/ggab261

Constraint of glacial isostatic adjustment in the North Sea with geological relative sea level and GNSS vertical land motion data

K.M. Simon [1,2] R.E.M. Riva[2] and L.L.A. Vermeersen[1,2]

[1] *NIOZ Royal Netherlands Institute for Sea Research, Korringaweg* 7, 4401 *NT Yerseke, the Netherlands. E-mail: k.m.simon@tudelft.nl*
[2] *Department of Geoscience and Remote Sensing, Delft University of Technology, Stevinweg* 1, 2628 *CN Delft, the Netherlands*

Accepted 2021 June 30. Received 2021 June 29; in original form 2020 November 25

SUMMARY

In this study, we focus on improved constraint of the glacial isostatic adjustment (GIA) signal at present-day, and its role as a contributor to present-day sea level budgets. The main study area extends from the coastal regions of northwestern Europe to northern Europe. Both Holocene relative sea level (RSL) data as well as vertical land motion (VLM) data are incorporated as constraints in a semi-empirical GIA model. 71 geological rates of GIA-driven RSL change are inferred from Holocene proxy data and 108 rates of vertical land motion from GNSS provide an additional measure of regional GIA deformation. Within the study area, the geological RSL data complement the spatial gaps of the VLM data and vice versa. Both data sets are inverted in a semi-empirical GIA model to yield updated estimates of regional present-day GIA deformations. A regional validation using tide gauges is presented for the North Sea, where the GIA signal may be complicated by lateral variations in Earth structure and existing predictions of regional and global GIA models show discrepancies. The model validation in the North Sea region suggests that geological data are needed to fit independent estimates of GIA-related RSL change inferred from tide gauge rates, indicating that geological rates from Holocene data do provide an important additional constraint for data-driven approaches to GIA estimation.

Key words: loading of the Earth; sea level change; satellite geodesy; Europe.

1 INTRODUCTION

Glacial isostatic adjustment (GIA) describes the process of the solid Earth surface and gravitational potential field perturbing and re-equilibrating in response to changing loads from ice sheets and glaciers and their redistributed ocean and shelf sea water equivalents. These perturbations in turn drive changes to the height of sea level over time (Walcott 1972; Farrell & Clark 1976; Peltier & Andrews 1976; Mitrovica & Milne 2003). At present-day, GIA can be driven by ice load changes that span millennial to decadal or even annual timescales, although the term GIA typically refers to deformations driven by the last glacial cycles (long-term GIA). Many recent studies that address ongoing present-day sea level and surface mass change have focussed on constraining the long-term GIA signal in order to remove its contribution from these measured variations and thereby better isolate the signals that are driven by recent changes to climate (e.g. Ivins *et al.* 2013; Caron *et al.* 2018; Whitehouse 2018).

Relative sea level (RSL) proxy data form the classical underlying data control for GIA models, and the fit of model predictions to these data typically either validate a particular model or are used as a basis for model revision. RSL proxy data generally consist of dated materials from coral reefs as well as sedimentary, biological, and archaeological records (e.g. Lambeck & Nakada 1990; Tushingham & Peltier 1992; Khan *et al.* 2019). RSL data points are also known as sea level indicators, and together their age, location, elevation, and indicative meaning can reconstruct the changing position of sea level through time in a given area (Shennan 2007; Shennan 2015). The indicative meaning is a property that relates the vertical position of a sea level indicator to a reference tidal level and expected vertical range of formation (Shennan 2007). Holocene RSL data have variable spatial and temporal distributions and are limited to coastal regions but have the advantage of being one of the only data types that constrain the changing magnitude and spatial pattern of GIA deformation over millennial timescales. By comparison, tide gauges record almost continuous changes to relative sea level at generally high accuracy (Holgate *et al.* 2013; Thompson *et al.* 2016); however, tide gauges are also subject to spatial coverage limitations and record only over the last several decades. Because of their time-series length, tide gauge data often contain significant signals related to recent changes in climate in addition to sea level changes driven by the long-term GIA response. In the last two decades, important additional constraint of GIA has been provided by satellite geodesy, namely, GNSS (Global Navigation Satellite Systems) and GRACE (Gravity Recovery and Climate Experiment), which measure vertical and horizontal motions of the

solid surface (e.g. Milne *et al.* 2001; Sella *et al.* 2002) and changes to the Earth's time variable gravity field (e.g. Tapley *et al.* 2004; Wouters *et al.* 2014), respectively. Unlike Holocene and tide gauge RSL data, these measurements can constrain GIA over continental interiors and record horizontal GIA deformations (GNSS only) but are limited to changes in the last 2–3 decades. As with tide gauge data, measurements from satellite geodesy often contain significant contributions from non-GIA processes, including tectonics and recent ice melt. Accurate separation of recent climate-driven signals from tectonic deformation and the relatively stable long-term GIA signal is needed to understand the role of various contributors to total present-day sea level and mass change budgets (Slangen *et al.* 2012; Rietbroek *et al.* 2016; Bamber *et al.* 2018; Caron *et al.* 2018).

In this study, geological RSL proxy data are employed in a somewhat different way than in traditional forward GIA models; instead of using the full time-varying RSL history, the Late Holocene data are used to infer present-day rates of relative sea level change. It is assumed that the rate of change of the GIA relaxation process over the Late Holocene (the time since ∼4 ka BP) has changed sufficiently slowly that the linear Late Holocene rate represents a reasonable approximation of the present-day rate of change. The inferred present-day rates are then inverted in a semi-empirical GIA model, alone and in combination with GNSS rates, to constrain the regional present-day GIA signal. As described in more detail in Section 4, the semi-empirical model combines present-day observations attributable to GIA with a prior model set of GIA model predictions such that the final product consists of data-driven maps of the GIA-induced component of several deformation fields at present-day (e.g. vertical land motion and relative sea level change). The output predictions therefore constrain the present-day GIA signal, but do no infer ice sheet or Earth model parameters. Previous studies (Simon *et al.* 2018) have also included GRACE data in the inversion, but we elect in this study to examine only the GNSS and RSL data sets since they are both pointwise data sets. To our knowledge, geological rates of RSL change, that is, rates derived from geological measurements of Holocene era materials, have not been used before as constraint in data-driven models of GIA. Given the power of Holocene RSL data as constraints in forward GIA models, it is desirable to explore the usefulness of translating these data into present-day rates for incorporation into data-driven GIA formulations that focus on estimation of present-day GIA signals. Specifically, the study objectives are: i) convert Holocene proxy RSL data into rates of present-day RSL change from GIA, ii) examine the utility of inverting the rates in a semi-empirical GIA model, and iii) apply the results in a sea level budget analysis in the North Sea.

The paper is structured as follows. Section 2 provides a summary of previous glacial and GIA modelling results for the region (including interpreted glaciation history and inferred Earth model parameters). Sections 3 and 4 respectively discuss the data and modelling methods used, while Section 5 presents the results including a validation in the North Sea region. Summary comments are presented in Section 6.

2 OVERVIEW OF REGIONAL GLACIAL HISTORY AND GIA MODELLING STUDIES

This work focuses on the estimation of the GIA signal at present-day and not on the constraint of GIA model parameters that describe aspects of ice sheet history or Earth rheology. However, the study area has been the focus of extensive GIA research over several decades. We therefore provide an overview of the glacial history and summarize some of the main findings of regional forward GIA modelling studies. In accordance with the regional nature of this study, this section summarizes only the regional glacial history of the study area. However, glacial isostatic adjustment is a global process with varying and complex regional expressions and present-day GIA signals are a response to both local and global ice sheet changes. That is, while the regional glacial ice sheet history is focussed on below, GIA models with regionally developed components also generally include a description of ice cover at the global scale to obtain more accurate GIA predictions.

The study area extends from northern Europe and the British Isles, across Scandinavia and northward to the Barents Sea and Russian Arctic (Fig. 1). During the last glaciation, there were three main glaciation centres in the region; at the last glacial maximum (LGM, ∼26–19 kyr BP), the British-Irish, Fennoscandian, and Barents Sea ice sheets coalesced to form the Eurasian Ice Sheet Complex (Patton *et al.* 2017). At its peak extent, the British-Irish Ice Sheet (BIIS) covered the northern British Isles and Ireland, was thickest in central and western Scotland, and coalesced across the northern North Sea basin with the Fennoscandian Ice Sheet (FIS). Although Eurasian ice cover extended farther south during a limited number of earlier glaciations (e.g. Lambeck *et al.* 2006), the LGM margins of the Eurasian ice sheet complex did not extend to the southern British Isles or the southern part of the North Sea basin. In Scandinavia, the FIS was thickest over northern Sweden and the Gulf of Bothnia and extended and thinned southwards to the Baltic Sea and Denmark. The Barents Sea ice sheet (BSIS) was a grounded marine based ice sheet centred over the Barents Sea and extended to northern Norway, Svalbard, Novaya Zemlya and Franz Josef Land at its margins. Together, the ice sheet complex contained at least 20 m of sea level equivalent at LGM, with the Fennoscandian Ice Sheet having the largest volume of the three sectors (∼14 m) and the British-Irish Ice Sheet the smallest (∼2 m) (Hughes *et al.* 2016). Observational data and glaciological modelling experiments suggest that neither growth nor retreat of the ice sheet complex was synchronous (Böse *et al.* 2012; Patton *et al.* 2016; Patton *et al.* 2017; Marks *et al.* 2018; Rinterknecht *et al.* 2018). Expansion of the three individual glaciation centres began after ∼35 kyr BP, with coalescence of the BIIS and FIS preceding BSIS expansion; maximum volume of the ice sheet complex was reached ∼22–21 kyr BP (Hughes *et al.* 2016). By 20 kyr BP, The British-Irish Ice Sheet was retreating from its margins and by 18 kyr BP had separated from the Fennoscandian Ice Sheet; between 19–15 kyr BP the BSIS retreated significantly. After 17 kyr BP and 15 kyr BP respectively, the BIIS and BSIS had decreased in volume by ≥1 m and ≥3 m sea level equivalent, and thus were contributing <1 m of global sea level equivalent to the ocean (Hughes *et al.* 2016). By 14 kyr BP, only the FIS had significant remaining volume in the region (∼6 m global sea level equivalent, Hughes *et al.* 2016). By 11 kyr BP, the FIS had shrunk further (∼1–2 m global sea level equivalent), and remnants of the BSIS existed over Svalbard, Franz Josef Land and Novaya Zemlya; deglaciation of the region was likely complete by ∼9 kyr BP (Carlson & Clark 2012; Hughes *et al.* 2016).

Understanding the regional land and sea level movements driven by these past glacial cycles has been the focus of numerous GIA modelling studies. For Scandinavia, Steffen & Wu (2011) summarized the results of several GIA modelling studies and indicated that these analyses suggest regional upper mantle viscosities of between 0.1–1 × 10^{21} Pa s and lower mantle viscosities approximately one to two orders of magnitude larger. Furthermore, they indicated

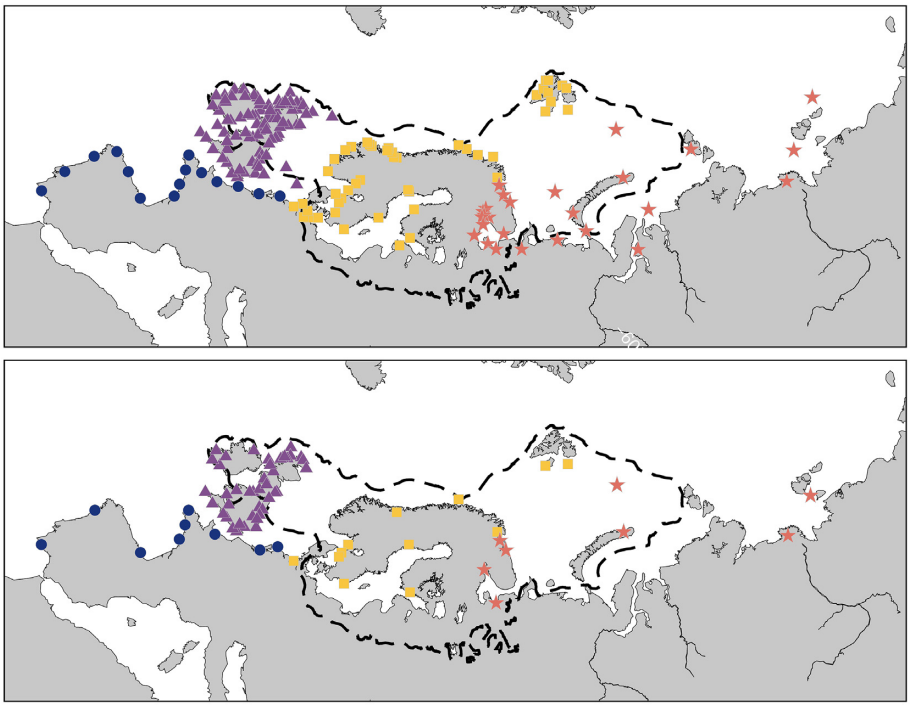

Figure 1. Relative sea level curves of the four regions. Upper panel—all RSL curves. Lower panel—those curves that fulfil the criteria for which to infer a rate of relative sea level change. Dark blue circles—European coastline (García-Artola *et al.* 2018; Meijles *et al.* 2018; Hijma & Cohen 2019); violet triangles—British Isles (Shennan *et al.* 2018); yellow squares—Scandinavia (Tushingham & Peltier 1993; Nordman *et al.* 2015); pink stars—Russian Arctic (Baranskaya *et al.* 2018). The approximate LGM boundary is shown by the black dashed line (Hughes *et al.* 2016).

that lithospheric thickness in Scandinavia likely varies from 80–200 km (Steffen & Wu 2011). More recent studies of Scandinavia infer values of upper mantle viscosity, lower mantle viscosity, and lithospheric thickness that may range from (or lie within) 0.34–3 $\times$ 10^{21} Pa s, 3–50 $\times$ 10^{21} Pa s, and 93–160 km, respectively (Zhao *et al.* 2012; Kierulf *et al.* 2014; Schmidt *et al.* 2014; Patton *et al.* 2017). In the British Isles region, studies indicate upper and lower mantle viscosity values within the ranges given for Scandinavia (3 $\times$ 10^{21} Pa s and 2 $\times$ 10^{22} Pa s respectively) but also suggest the presence of a thinner lithosphere of ∼71 km (Bradley *et al.* 2011; Kuchar *et al.* 2012). In the more northern part of the study area, around the Barents Sea region, Auriac *et al.* (2016) summarized the predictive ability of six ice sheet models; the selected best-fitting models infer respective upper and lower mantle viscosities of 0.2–2 $\times$$10^{21}$ Pa s and 1–50 $\times$ 10^{21} Pa s and lithospheric thicknesses of 71–120 km. Both Root *et al.* (2015) and Patton *et al.* (2017) have inferred regional Earth parameters that are within the ranges given by Auriac *et al.* (2016).

3 DATA

3.1 Geological RSL data: availability and selection criteria

The study area has a good availability of Holocene RSL data, much of which has been published recently following consistent data reporting protocols (Hijma *et al.* 2015; Khan *et al.* 2019). Following published data sources, the study area is divided into four regions (Fig. 1): i) the European coastline (García−Artola *et al.* 2018; Meijles *et al.* 2018; Hijma & Cohen 2019), ii) the British Isles (Shennan *et al.* 2018), iii) Scandinavia including Svalbard (Tushingham & Peltier 1993; Nordman *et al.* 2015), and iv) the Russian Arctic (Baranskaya *et al.* 2018).

In all of the data sets used here, spatially adjacent RSL data points are grouped into regional RSL curves that describe the time-varying changes to RSL within a given region (Fig. 1). The European coastline has a total of 15 RSL curves, with 13 along the Atlantic coastline (García−Artola *et al.* 2018) and an additional two sites in the Netherlands along the North Sea coastline (Meijles *et al.* 2018; Hijma & Cohen 2019). The British Isles database has 86 RSL curves (Shennan *et al.* 2018), Scandinavia has 47 RSL curves, and the Russian Arctic has 26 RSL curves (Baranskaya *et al.* 2018). Within most of the databases, individual sea level indicators are classified as being either sea level index points (SLIPs) or as marine or terrestrial limiting data. Sea level index points define the position of sea level at a distinct point in space and time (with uncertainties), whereas limiting data cannot be related to past tidal levels and therefore only provide lower bounds (marine limiting) or upper bounds (terrestrial limiting) on the position of sea level (Hijma *et al.* 2015).

In order to calculate a geological rate of RSL change, a given RSL curve must have two or more data points within the specified time interval ($\leq$4 kyr BP). The selected time interval considers not only the time frame in which linearity of the GIA process is likely reasonable, it also reflects a natural cut-off within some data sets; for example, along the parts of the North Sea coast, earlier Holocene sea level basal peat indicators in younger time are typically replaced by later Holocene salt marsh indicators (Vermeersen *et al.* 2018; Hijma & Cohen 2019) and in general there has been debate over the reliability and quality of interpreted sea level signals over the last ∼4000 yr (e.g. Bungenstock & Weerts 2010). Another criterion is that, for the European coastline and British Isles data, all selected points must be classified as SLIPs. This constraint is applied because SLIP data in these regions are ample and are best suited to this study (i.e. they will provide rates more consistent with vertical rates derived from GPS); however, terrestrial and marine limiting data remain valuable

constraints for GIA studies. The 'SLIP only' constraint is not applied to the Scandinavian RSL information because these data have not been published following the same standardization as the other more recent data sets and do not include the data point type classification. This means that, for Scandinavia, the derived rates should be considered approximate; for now, we account for this by increasing the measurement uncertainty on the RSL data by a factor of two. These rates can be revisited when the Scandinavian data are publicly available following the same protocols as the other data sets; a new sea level database for the Baltic Sea region is already in progress (Klemann *et al.* 2018; Rosentau *et al.* 2021, QSR, in revision). An exception to the limitation of the Scandinavian RSL information used here is the reappraisal of the RSL curve from Ångermanland in central Sweden published by Nordman *et al.* (2015); these data are reported with more detailed information including the material type and higher precision radiocarbon and varve ages. The 'SLIP only' constraint is likewise not applied to the Russian Arctic data as most curves there have fewer SLIPs in the later Holocene than either the European coastline or British Isles data. However, for the Russian Arctic data, if the computed rate is determined with only upper limiting data and/or lower limiting data, it is excluded from consideration as these rates will represent upper or lower bounds only.

3.2 Data corrections

Over millennial timescales, RSL curves probably are not strongly influenced by shorter term climate change signals that influence tide gauges and satellite geodetic measurements. However, several processes can contribute to changes recorded in Holocene relative sea level data (e.g. Shennan *et al.* 2012 their fig. 1), of which glacial isostatic adjustment is only one. The sea level data may for example contain other significant contaminating (non-GIA) signals due to tectonics, sediment compaction and barystatic sea level change. As discussed below, corrections will differ between regions, data sources, and in the case of some of the more modern databases, the user's choice of starting RSL position (corrected or uncorrected).

3.2.1 Tectonics

Sea level can be influenced by both longer-term (traditional) tectonic signals as well as short-term (neo-)tectonic activity; it is therefore worth evaluating whether the sea level data examined here can be expected to contain significant tectonic signals. Region 1, the European coastline, includes the Atlantic coastline of Portugal, Spain, and France, as well as the North Sea coastline in the Netherlands. The northern coastline of Spain is a passive margin dating to the Mesozoic, and much of the French sea level data originates from the Armorican Massif; both regions are generally considered to be tectonically stable on Holocene timescales (Boillot *et al.* 1979; Morzadec-Kerfourn 1995; Lambeck 1997; García-Artola *et al.* 2018). There is observed seismicity and neotectonic activity along the Portuguese coastline (Leorri *et al.* 2012, García-Artola *et al.* 2018), although some studies have suggested that along the southern Portuguese margin recent tectonic movements are small or negligible (Delgado *et al.* 2012).

On the other hand, the Dutch, German and SW Danish coastlines lie along the southern rim of the North Sea basin, a basin formed by Jurassic-early Cretaceous rifting and a subsiding sedimentary depocentre with active deposition throughout the Cenozoic including the Quaternary period (e.g. Cloetingh *et al.* 2007; Phillips *et al.* 2017; Westaway 2017). Some tectonic subsidence around the boundaries of the North Sea is expected, with subsidence rates generally increasing into the basin (Vink *et al.* 2007; Kiden *et al.* 2008) although constraining the magnitude and regional variability of the signal is difficult. There have been numerous studies that discuss the separation of isostatic and tectonic signals in sea level data from the Netherlands. Kooi *et al.* (1998) and Vink *et al.* (2007) estimate an average tectonic subsidence rate of -0.142 mm yr^{-1} for the western Netherlands. In the northeastern Netherlands and around the German Bight, the tectonic subsidence estimates decrease to approximately -0.05 mm yr^{-1} (Vink *et al.* 2007). These regional estimates are in general agreement with those of Kiden *et al.* (2002) (~ -0.06 to -0.16 mm yr^{-1}). In summary, while it seems that the tectonic signal along the Dutch coastline is both considerably smaller than isostatic movements (Kiden *et al.* 2002; Meijles *et al.* 2018) and can be challenging to constrain (both magnitude and operating timescale), various studies do point towards a non-negligible tectonic component of subsidence that may be on the order of up to -0.1 mm yr^{-1}.

In Region 2, the British Isles, vertical tectonic motions are generally cited as being negligible during the Holocene period (Shennan & Horton 2002; Teferle *et al.* 2009; Shennan *et al.* 2012) although in southeast England, evidence of longer-term signals on the order of ~ 0.1 mm yr^{-1} driven by isostatic uplift from erosion (Bridgland & Schreve 2009; Shennan *et al.* 2012) and neotectonic signals (Teferle *et al.* 2009) have been reported.

In Scandinavia, Region 3, the vertical deformation signal in particular is likely dominated by glacial isostatic adjustment. Milne *et al.* (2001) presented a 3-D map of crustal motions in Scandinavia derived from GPS (Global Positioning System) measurements. Removing best-fit GIA model predictions from the observed deformation field, the authors suggested that the residual vertical motion signal may be attributable to tectonics, with the inferred signal not exceeding ± 1 mm yr^{-1} for most of the region. For the majority of the Scandinavian RSL locations, this uncertainty is less than the computed uncertainty of the Late Holocene RSL rate (Section 3.3, Table S1). Neotectonic activity in the form of intraplate seismicity (associated with a combination of postglacial rebound and ridge-push from the North Atlantic region) is observed throughout Scandinavia (Steffen & Wu 2011).

Region 4, the Russian Arctic, is tectonically complex, with numerous faults and tectonic boundaries. Much of the sea level data come from the Baltic Shield, the Russian Plate, the Franz Josef Land flood basalt massive, and the Siberian Platform (Baranskaya *et al.* 2018). Both the Baltic Shield in the western portion of the region around the Kola Peninsula as well as the Laptev Sea in the eastern part of the region and part of the Siberian platform experience some degree of active tectonic movements (Baranskaya *et al.* 2018). Anomalously high sea level positions in western Siberia could also be attributable to tectonic uplift (Baranskaya *et al.* 2018).

In summary, a tectonic correction is not applied to the data from the Atlantic part of the coastline from Region 1, to the British Isles data, or the Scandinavian data, because the regions are assumed to be relatively tectonically stable over the later Holocene. A tectonic subsidence correction is applied to the two sea level curves from the Dutch North Sea coast (-0.14 ± 0.07 mm yr^{-1} for Rotterdam and -0.05 ± 0.025 mm yr^{-1} for the Wadden Sea and German Bight); the 50 per cent uncertainty is ad-hoc and accounts for the considerable uncertainty that may be associated with regional estimates of long-term sedimentary basin subsidence (e.g. Hijma & Kooi 2018). For the Russian Arctic, a correction for neotectonics may well be relevant at some locations although quantitative constraints are sparse

and tectonic correction values are not provided in Baranskaya *et al.* (2018).

3.2.2 Compaction and other local effects

Local processes, such as sediment compaction, can also influence the interpreted position of past sea level. García-Artola *et al.* (2018) do not explicitly incorporate uncertainty in the RSL vertical position associated with sediment compaction, although to minimize the influence of compaction, they only consider basal dates for the freshwater limiting data. Kiden *et al.* (2002) indicate that compaction of underlying deposits in the region is considered negligible on Holocene timescales. However, the latest Holocene data from the RSL curve from the Wadden Sea is likely influenced by sediment compaction and/or raised groundwater table effects (Meijles *et al.* 2018). For this reason, as suggested by Meijles *et al.* (2018), the later Holocene data from the Wadden Sea (after 2 kyr BP) may be better interpreted as terrestrial limiting data rather than sea level index points; to account for this uncertainty in interpretation, we increase the vertical uncertainty on the Wadden Sea data by a factor of two and indicate (visually only) that these data may be terrestrial limiting (Supporting Information Fig. S1). Sediment compaction likely affects some of the samples from the British Isles (Shennan & Horton 2002, Shennan *et al.* 2018). In their database, Shennan *et al.* (2018) included estimated corrections for sediment compaction and tectonics—it is the corrected RSL positions that have been used for the rate calculations. For the RSL data from Ångermanland in Scandinavia, Nordman *et al.* (2015) indicate that the error associated with compaction is likely negligible, and thus do not incorporate a compaction correction. In the Russian Arctic RSL database, there are likewise no compaction corrections included and Baranskaya *et al.* (2018) indicate that most samples from this region are from non-sedimentary sources and therefore are not expected to experience significant compaction.

3.2.3 Barystatic sea level change

Finally, because Holocene RSL curves record a combination of change due to (local) crustal displacement from glacial isostatic adjustment and the global effect of barystatic sea level rise due to deglaciation, some studies consider a correction for barystatic sea level change to isolate better local crustal movements in sea level records. Unlike tectonics and sediment compaction, which can locally vary in value, barystatic sea level change is spatially uniform and varies only in time. This study however considers both the local and global effects on sea level change to be part of the GIA process and thus no correction for barystatic (often formerly eustatic, Gregory *et al.* 2019) sea level change is required.

3.3 RSL rate calculation

There are various ways to compute trends of Holocene RSL change (Ashe *et al.* 2019). Here, all rates are calculated with a linear fit to the data points of $\leq$ 4 kyr BP age, with linearity of the RSL curves considered to be a reasonable assumption for later Holocene data. Specifically, the rates are computed using iteratively reweighted least squares to limit the influence of outliers in the data set. At present, only the elevation uncertainties are used in the trend calculations although the age uncertainties can be significant at some locations. However, tests that incorporated the age uncertainties indicated that the calculated trends were not strongly sensitive to their inclusion. Plots of the sea level data and the computed trends are provided in the Supporting Information (Figs S1–S4). Computed rates with at least 2σ significance or failing that, calculated uncertainties of ≤ 0.5 mm yr^{-1}, are included in the analysis. Out of the original 175 RSL curves, the applied criteria yield a total of 71 rates for consideration (9 for the mainland European coastline, 42 for the British Isles, 12 for Scandinavia and 8 for the Russian Arctic; Fig. 1, Supporting Information Table S1).

Along the mainland European coastline, inferred rates of present-day relative sea level change are small, and range from approximately 1.0 mm yr^{-1} of sea level rise along the North Sea coastline and German Bight to 0.1 mm yr^{-1} of sea level fall in Iberia (Fig. 2, Supporting Information Table S1). In the British Isles, the rates range from 1.6 mm yr^{-1} of sea level fall in central and western Scotland and up to 1.8 mm yr^{-1} of sea level rise in southeastern England. The rates in this region are also characterized by the smallest estimated uncertainties. Across Scandinavia, sea level change rates vary from 0.4 mm yr^{-1} of sea level rise along the northern coastline of Germany to 10.9 $\pm$ 0.5 mm yr^{-1} of sea level fall at Ångermanland, near the centre of the former Fennoscandian Ice Sheet. In the Russian Arctic, the calculated rates all predict sea level fall that ranges from -0.3 to -3.2 mm yr^{-1}.

As a means of checking the computed geological rates, they are compared with RSL rates at co-located tide gauges from the Permanent Service for Mean Sea Level (PSMSL; Holgate *et al.* 2013; PSMSL 2019). The comparison shows that tide gauge derived sea level change is consistently higher (by $\sim$1 mm yr^{-1}) than sea level change derived from the geological data (Fig. 3). This result is generally consistent with the results of Shennan & Horton (2002), who showed a similar comparison using data from 17 sites within the British Isles only and also found an offset on the order of $\sim$1 mm yr^{-1}. The $\sim$1 mm yr^{-1} offset is consistent with 20th century GMSL change (Dangendorf *et al.* 2017), a signal which will not be captured by the geological sea level data. The selected PSMSL data uses time-series of $\geq$ 50 yr length and records that are $\geq$ 70 per cent complete. The tide gauge sea level trends shown in Fig. 3 are computed using the Hector software package with a generalized Gauss Markov noise model (Bos *et al.* 2013).

3.4 Vertical land motion data

Rates of vertical land motion are derived from GNSS measurements, specifically GPS, and provide additional constraint for the model inversion. The GPS-measured VLM rates are from the Nevada Geodetic Laboratory (Blewitt *et al.* 2016) and from the study of Kierulf *et al.* (2014) (Scandinavia only) and are shown at the 2σ significance level (108 sites, Fig. 4). The selected rates span 1996–2016 and have been corrected for present-day mass effects (melt from Greenland, Antarctica and glaciers and ice caps) following the correction from Simon *et al.* (2018, their fig. 3). Specifically, Greenland Ice Sheet mass loss is estimated from 1993 to 2014 using surface mass balance estimates from RACMO2.3 (Noël *et al.* 2015) and ice discharge with a constant acceleration of 6.6 Gtyr^{-2} (van den Broeke *et al.* 2016). Antarctic Ice Sheet mass loss is estimated over the same period using RACMO2.3p1 and a constant acceleration in ice discharge of 2 Gtyr^{-2} (van Wessem *et al.* 2016). The elastic correction ranges in magnitude from $\sim$0.2–0.5 mm yr^{-1} throughout the study area with the largest contribution coming from Greenland Ice Sheet melting. For both the Holocene RSL data and the GPS data, it may also be important to consider local vertical deformation due to anthropogenic activity such as mining in Great

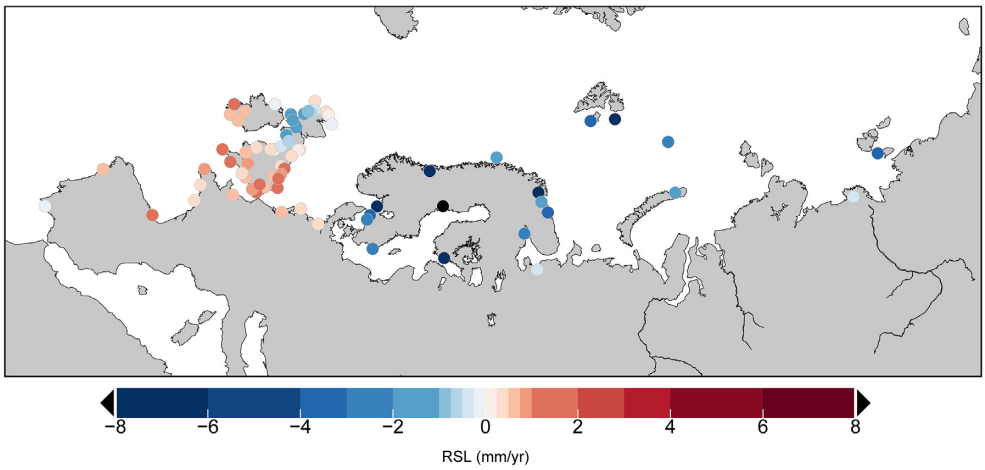

Figure 2. Inferred rates of present-day RSL change across the study area. Note uneven scale.

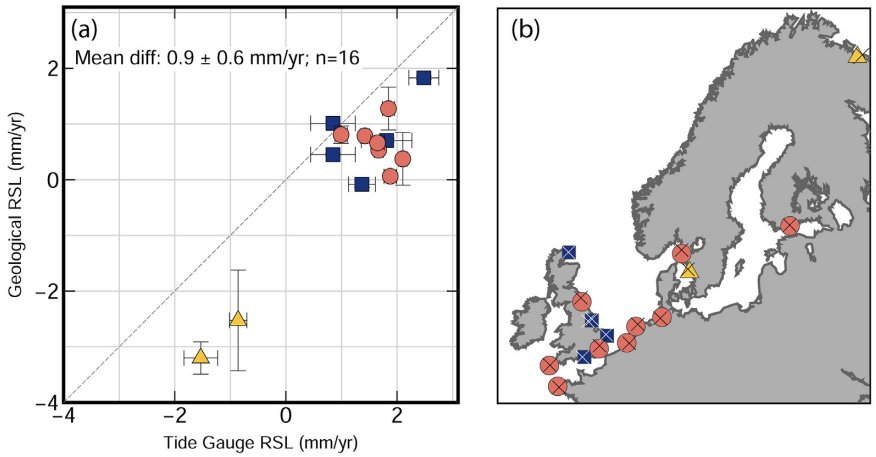

Figure 3. (a) Inferred rates of geological RSL change versus RSL rates derived at collocated tide gauges (TG) within the study area. (Pink circles: 100+ yr TG data; yellow triangles: 75+ yr TG data; dark blue squares: 50+ yr). The tide gauge derived rates are on average 0.9 mm yr^{-1} higher than the inferred geological rates. (b) TGs [coloured symbols as in (a)] with collocated geological RSL sites superimposed as crosses.

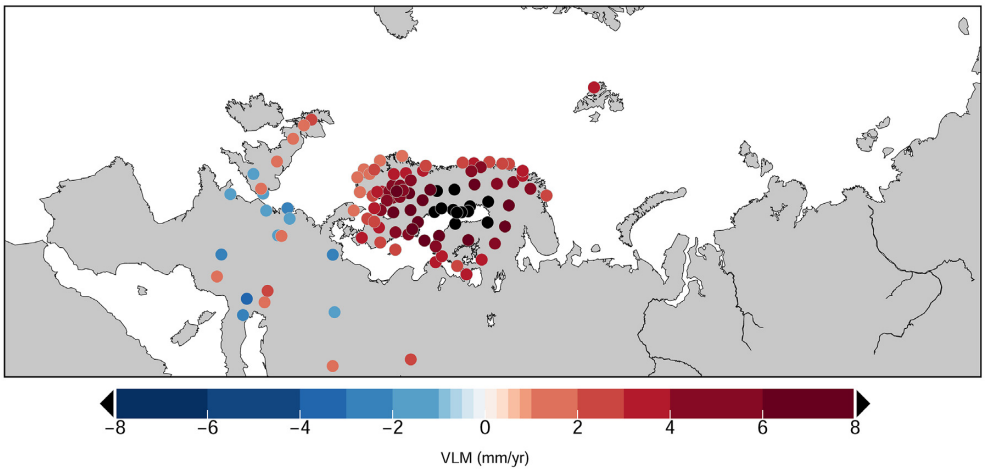

Figure 4. Rates of vertical land motion from GPS used in the inversion (108 sites). Rates of VLM from GPS from the Nevada Geodetic Laboratory (Blewitt *et al.* 2016) and Kierulf *et al.* (2014) (Scandinavia only), shown at the 2σ significance level. The rates span 1996–2016 and have been corrected for present-day mass effects (melt from Greenland, Antarctica and glaciers and ice caps).

Britain (Humphries 2001; Bell *et al.* 2005) and gas extraction in the northern Netherlands (de Waal *et al.* 2015; Fokker *et al.* 2018). However, corrections for local anthropogenic activity have not been applied here for the time being. In the input VLM data set used, there are relatively few subsidence measurements, and fewer still that record subsidence rates in excess of 3 mm yr^{-1}; the localized effect of anthropogenic activities is therefore likely small in the inversion. For the two locations along the Dutch North Sea coastline, the small tectonic subsidence correction applied to the RSL data is also applied to the corresponding GPS rates.

4 METHOD

Forward modelling studies that aim to describe the GIA process typically select a body of observational constraints against which to evaluate and refine a coupled model description of the ice sheet history and Earth structure. Ice sheet models are constrained by reconstructions of retreat history, estimates of maximum ice volume, inferences of glacial flow directions and areal extent of past ice sheets; some GIA models include explicit ice sheet models covering ice mechanics and incorporating glaciological and climatological information (Tarasov *et al.* 2012; Gowan *et al.* 2016), while others use the fit to RSL proxy data to describe how ice volume and thickness varied in time and space without specifically incorporating ice physics (Peltier 2004; Peltier *et al.* 2015). Earth model formulations likewise vary. 1-D radially varying Maxwell viscoelastic models are commonly used, although models that allow for 3-D Earth structure and/or different parametrizations of mantle rheology have been increasingly prevalent in recent years (e.g. van der Wal *et al.* 2013; Li & Wu 2019; van Casteren 2019). The benefit of the forward modelling approach is the ability to incorporate and therefore constrain ice sheet and Earth parameters; the associated limitation is that the uncertainties associated with model parametrizations are carried forward into the model predictions leading to non-unique solutions (e.g. Whitehouse 2018). Conversely, semi-empirical type models do not offer direct constraints on model parameters (e.g. Riva *et al.* 2009; Hill *et al.* 2010; Simon *et al.* 2017), but do, through a data-driven approach, minimize the uncertainties inherent to the traditional forward modelling approach.

The least-squares adjustment methodology used in this study is based on Hill *et al.* (2010) and Simon *et al.* (2017). The method simultaneously inverts the data constraints with a priori GIA model information and minimizes the misfit to both the data and prior model inputs; the data and prior inputs are also weighted using variance component estimation as described in Simon *et al.* (2017). The prior model set consists of 96 model forward GIA model runs that includes predictions of present-day deformation rates. Two ice sheet scenarios are used: ICE-6G (Peltier *et al.* 2015) and the version of the ANU ice sheet model for the British Isles and Scandinavia (Lambeck *et al.* 2010). The second scenario includes the North American component of Simon *et al.* (2016) and ICE-5G (Peltier 2004) elsewhere. The Earth models in the prior set are three-layer radial Maxwell viscoelastic models, with upper and lower mantle viscosities that range from 0.2 to 2 $\times$ 10^{21} and 1 to 60$\times$$10^{21}$ Pa s, respectively. Because the two ice sheet models were each tuned to be valid with a particular description of Earth structure and rheology, coupling the ice sheet models with a large set of Earth models will create some ice-Earth model combinations that generate predictions inconsistent with observational constraints. However, the goal of the prior model set is not solely to generate best-fit GIA predictions, it is rather to create a range of predictions that bracket plausible GIA deformation. Three data combinations with the a priori model set are considered: inversion of the VLM data only (model G1), inversion of the geological RSL data only (G2) and inversion of both the VLM and geological RSL data sets (G3). The G1 model is similar to the D1 model of Simon *et al.* (2018), which also used measurements from GPS as the only data constraint in the inversion. The G1 model inverts a smaller subset of VLM measurements than the D1 model; however, the average predicted difference between the models is < 0.2 mm yr^{-1} throughout the study area for both the VLM and RSL predictions.

5 RESULTS

5.1 Regional GIA predictions

The predicted rates and uncertainties of GIA-related RSL change at present day for models G1-G3 are shown in Fig. 5. Analogous plots for predicted vertical land motion are shown in Supporting Information Fig. S5. The predicted signals of the three models show broad similarities, with RSL fall predicted over central Scandinavia and the British Isles and RSL rise predicted in the southern British Isles and along much of the northern European coastline. There are also several differences, including the location of peak RSL fall in Scandinavia—the G2 model predicts a more south-westerly peak in RSL fall whereas including the GPS rates (G1 and G3) places the peak RSL fall more directly over the central Gulf of Bothnia. Over the British Isles, inclusion of the geological RSL data (G2, G3) reduces the size of the region of RSL fall in the north, with the transition from RSL fall to RSL rise occurring farther north than in model G1. Because consideration of tectonic signals may be required for the Russian Arctic region, we also downweighted the RSL data from the Russian Arctic region in the inversion; the predicted deformation patterns over Scandinavia, northern Europe and the British Isles were not particularly sensitive to the downweighted Russian Arctic rates and the test had negligible effect on the North Sea validation presented in the next section.

Although RSL change is not the direct inverse of VLM, the predicted pattern of VLM uplift (Supporting Information Fig. S5) broadly mirrors the predicted pattern of RSL fall. The GPS site at Umeå, Sweden, is located approximately at the centre of Scandinavian uplift (~63.6 N, 19.5 E). The empirical model predictions should be able to reproduce GPS-measured uplift here, which in our input is 9.7 $\pm$ 0.5 mm yr^{-1}. Both the G1 and G3 models succeed in this respect, with predicted uplift rates of 9.3 $\pm$ 0.2 and 9.2 $\pm$ 0.5 mm yr^{-1}, respectively. At 8.5 $\pm$ 0.8 mm yr^{-1}, the G2 model underpredicts vertical land motion at this location; this underprediction is a consequence of the sparser, more loosely constrained last 4 kyr RSL inputs for the Scandinavian region and may also indicate that the assumption of linear change during the Late Holocene does not hold for central Scandinavia. Moreover, in comparison to the GNSS data, the peak uplift of the G2 model at >10 mm yr^{-1} is too large, and located too far to the southwest in the region (Fig. 5, Supporting Information Fig. S6). The predicted G1 and G3 vertical velocities are similar to the maximum rates in the Scandinavian land uplift model of Vestøl *et al.* (2019).

The average absolute values of the residuals for the VLM data (e_{vlm}) are (0.76, 1.70, 0.81) mm yr^{-1} for the G1–G3 models (Supporting Information Fig. S6). The average absolute values of the residuals for the RSL data (e_{rsl}) are (0.82, 0.54, 0.66) mm yr^{-1} for the G1–G3 models (Supporting Information Fig. S7). The G1 model fits the VLM observations the best ($e_{vlm} = 0.76$ mm yr^{-1}) and the

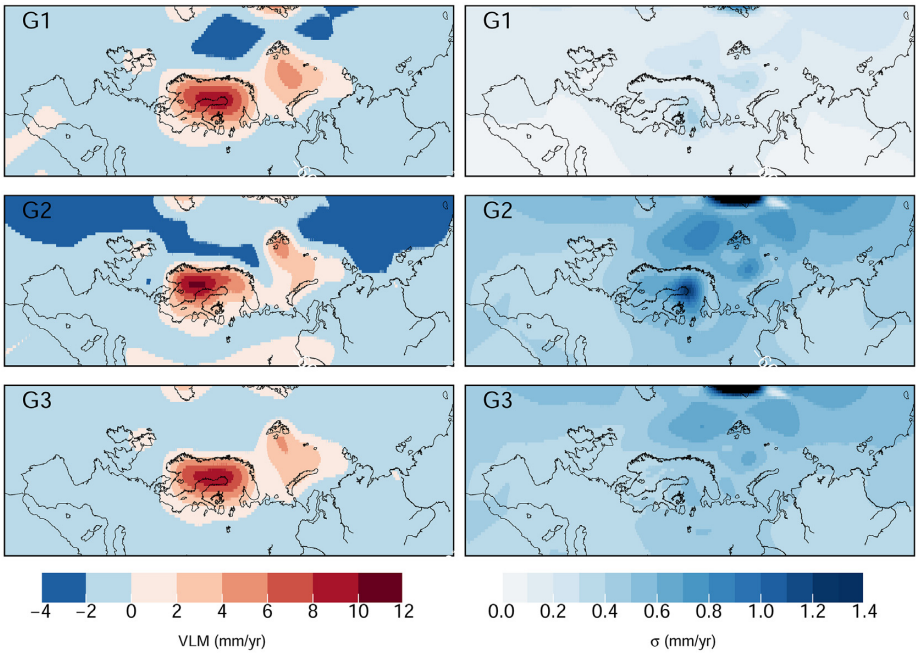

Figure 5. Model predictions of GIA-induced present-day RSL change and uncertainty using VLM data (G1), geological RSL data (G2) and both VLM and geological RSL data (G3) as inputs. In regions without significant data coverage (see Figs 2 and 4) the predictions will not be well constrained by data.

RSL proxy rates the worst ($e_{\mathrm{rsl}} = 0.82$ mm yr^{-1}). In particular, the VLM residuals are inversely proportional to data coverage, with larger residuals present over the British Isles and smaller residuals over Scandinavia where GPS coverage is dense. Similarly, the G2 model predictions fit the RSL rates the best ($e_{\mathrm{rsl}} = 0.54$ mm yr^{-1}) and the VLM rates the worst ($e_{\mathrm{rsl}} = 1.70$ mm yr^{-1}). In G2, the rates of vertical land motion show a zone of strong overprediction in southern and western Scandinavia which is mirrored by a similar zone of underprediction in northern and eastern Scandinavia. This misfit pattern is largely the result of a lack of (low uncertainty) RSL proxy rates in the region. Inclusion of the Late Holocene sea level rates derived from the geological proxy data in G2 and G3 decreases the RSL residuals most notably in the British Isles region, where current RSL data coverage is densest. As expected, the best overall fit to both data sets, RSL and VLM, is obtained for the G3 model (e_{vlm} and e_{rsl} of 0.81 and 0.66 mm yr^{-1}, respectively).

5.2 Validation in the North Sea

In this section, we consider a test to evaluate the robustness of each of the model predictions. Along the North Sea coastline, predictions of present-day RSL change extracted from various regional and global GIA models indicate deviating patterns of RSL rise and fall (Vermeersen *et al.* 2018; Fig. 6), making the region an interesting candidate for a data-driven scenario. Lateral variations in lithospheric thickness, which are expected between Scandinavia, the British Isles and the North Sea Basin in between, may further complicate the interpretation of regional 1D GIA model predictions (Section 2).

The test follows a similar analysis from Simon *et al.* (2018) in which two categories of independently derived rates of RSL change from GIA are compared. The first category of RSL rates are the predictions of the G1-G3 models. The second category of RSL rates are derived from correcting measured rates of RSL change from tide gauges for non-GIA processes. Following Frederikse *et al.* (2016), RSL rates at 12 PSMSL tide gauges in the North Sea (Fig. 7) are corrected for present-day mass effects and ocean dynamics to yield a tide-gauge derived estimate of the GIA component of RSL change (Fig. 8). However, while the processes of present-day mass loss and ocean dynamics are removed from the total tide gauge rates, local sea level variability may still be present and therefore represents a potential source of uncertainty in the inferred GIA contribution. The signal from ocean dynamics is based on an apparent correlation between the open ocean steric signal in the Bay of Biscay with North Sea level variability—the strong correlation between the two regions allows the Bay of Biscay open ocean estimates to be used as a proxy to describe the steric-induced sea level change in the North Sea (Frederikse *et al.* 2016). The present-day mass estimates are obtained by solving the elastic sea level equation for present-day melt scenarios for Greenland, Antarctica, and glaciers and ice caps.

The corrected tide-gauge estimates provide independent values of GIA against which the semi-empirical model predictions (G1–G3) can be compared. Fig. 8 shows that inclusion of the geological RSL data provides a better fit to the tide-gauge derived rates, with the G3 model providing the best fit overall ($\chi^2 < 1$). Improved fits with respect to G1 are particularly notable at North Shields and Lowestoft in the British Isles, a region where there are abundant good quality RSL data. The improved agreement between the two independent estimates suggests that proxy RSL data can provide useful constraints in semi-empirical models, particularly in regions with good spatial coverage.

6 DISCUSSION AND CONCLUSIONS

We have derived 71 proxy rates of RSL change due to long-term GIA over northern Europe and Scandinavia. In three of the four regions of the study area, the RSL data have been recently updated in an attempt to report sea level data following consistent protocols (e.g. Hijma *et al.* 2015). In general, the derived trends are consistent with expectations: the rates indicate strong GIA-induced sea level

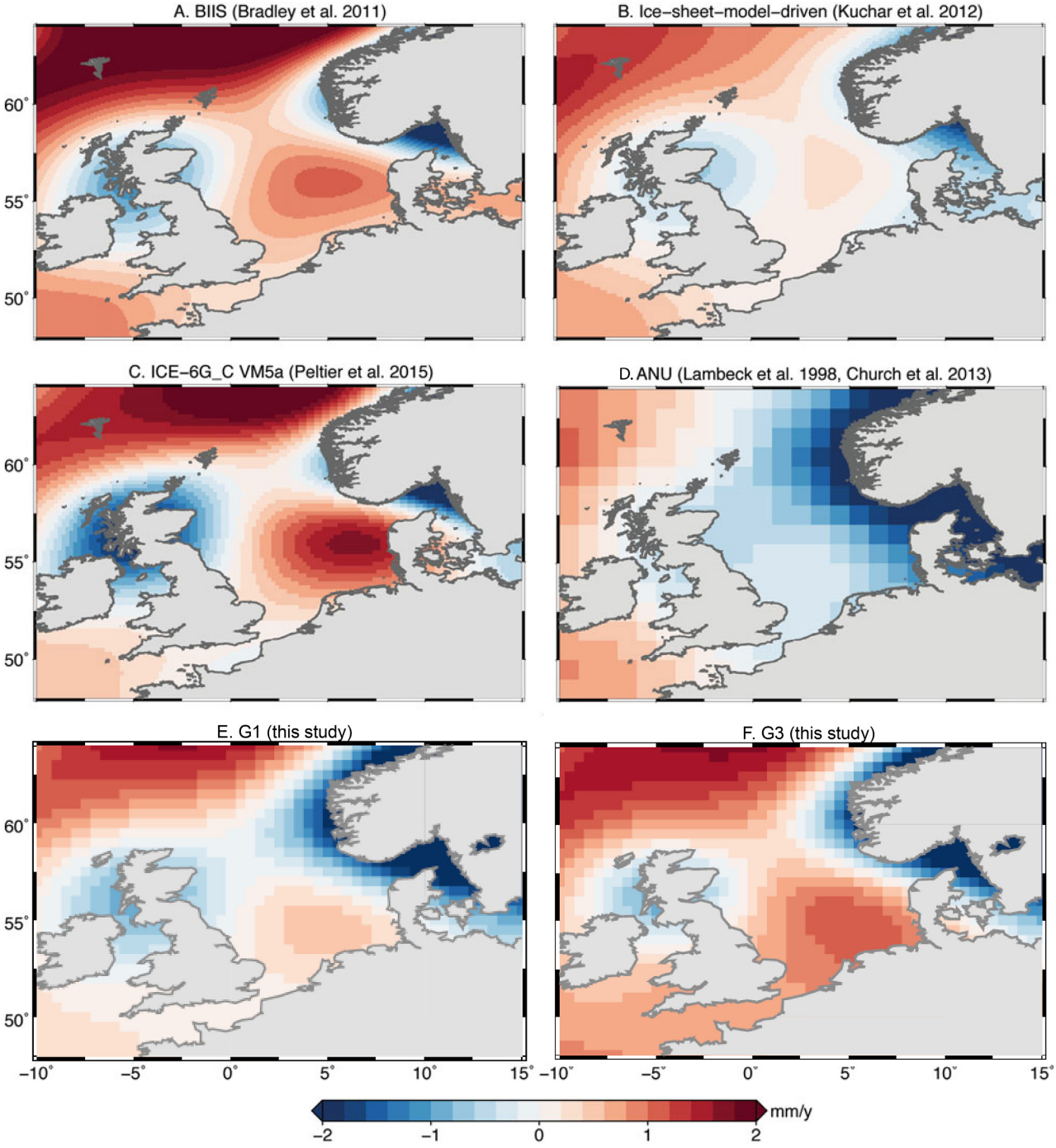

Figure 6. GIA model comparison: predictions of present-day RSL change due to GIA in the North Sea from various regional and global models and using different methodologies indicate variable patterns of RSL rise and fall (panels a–d are adapted from Vermeersen *et al.* 2018; panels e and f are from this study). The prior model information in panels (e) and (f) include the ice sheet information of panels (c) and (d).

fall in central Scandinavia, moderate sea level fall in the northern British Isles, and weak sea level rise along much of the northern European coastline.

There are limitations of the current study that future research can address. Specifically, when updated data sets for RSL data in Scandinavia, and the North Sea and Baltic Sea regions become available, the geological rates should be revisited to quantify the impact of the improved data constraints; new or updated data sets may provide better spatial coverage and/or smaller data uncertainties. As well, different models for rate calculations exist and could be explored (Ashe *et al.* 2019), although later Holocene data are probably less sensitive to modifications in the assumption of linearity than earlier Holocene data. And, while the calculated rates may have some sensitivity to the details of the rate calculation, the rates are likely most sensitive to the robustness of applied corrections for non-GIA signals. This is particularly true in regions outside of central Scandinavia (where the signal will be dominated by GIA) such as around the southern North Sea coastline where GIA and non-GIA signals

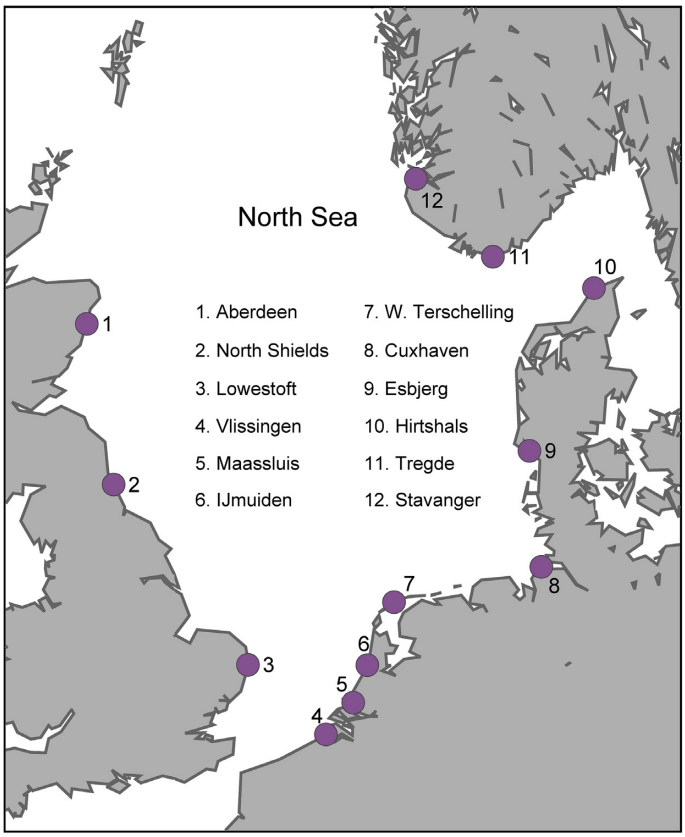

Figure 7. Locations of 12 tide gauges around the North Sea.

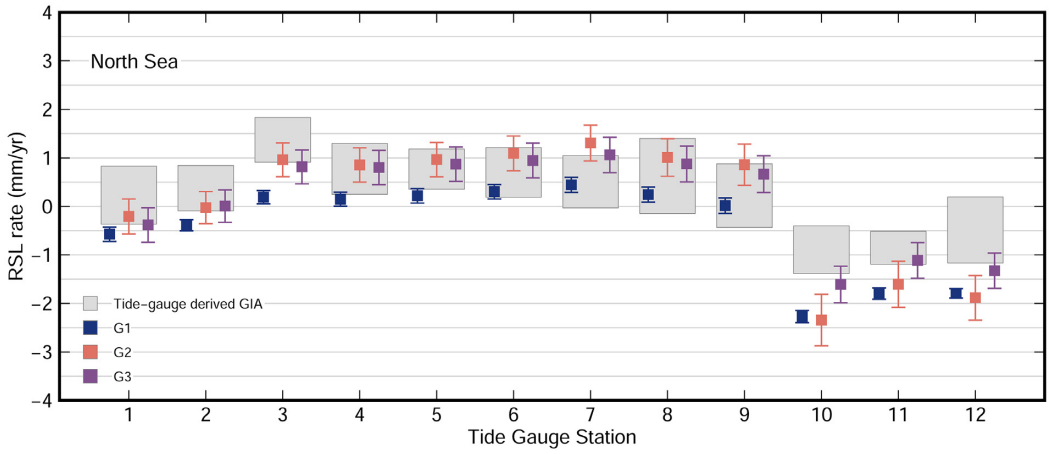

Figure 8. Comparison of GIA-related RSL change derived from tide gauges (grey boxes) to predictions of the semi-empirical model (G1–G3, coloured squares) at 12 North Sea stations.

are of the same magnitude. For example, the tectonic subsidence signal here is challenging to constrain and therefore difficult to separate with confidence from the GIA subsidence signal. Finally, the derived rates in the Russian Arctic do not include a correction for tectonic movements. However, a tectonic correction may well be required at some sites in this region, so within the context of GIA, the derived rates should be interpreted with some caution.

What we have implemented is a first attempt at using proxy rates of Late Holocene RSL change derived from geological sea level data as a constraint in a semi-empirical GIA model. This approach differs from the usual use of Holocene sea level data in GIA models: in most GIA studies, geological sea level measurements have been used as pointwise, space–time varying data to validate GIA models (i.e. to evaluate to what extent GIA models adequately capture deglaciation-related sea level change). In contrast, here we have used the youngest part of the geological data sets to infer proxy rates of sea level change as a way to calibrate present-day rates predicted by GIA models. Such an approach may be useful to explore further, as data-driven approaches are increasingly used to constrain the present-day GIA signal. The typical focus of data-driven predictions is logically to use contemporary timescale data sets, but these data often include large signals from present-day ice

melting and/or continental hydrology. While geological rates may also contain contaminating signals from various processes that require correction (Section 3.2), they will, in strong contrast to GNSS and tide gauge data collected during the 20th and 21st centuries, be relatively free of signals from recent changes to climate. The geological proxy rates thus provide a unique data set with which to complement or validate existing data-driven approaches that use satellite era rates of change.

ACKNOWLEDGEMENTS

This work is funded by the Netherlands Organisation for Scientific Research (VIDI Grant No. 864.12.012 and GO Programme Grant ALWGO.2017.005). We thank Kim Cohen and Volker Klemann for constructive reviews that helped to significantly improve the manuscript.

DATA AVAILABILITY

As described in the text, the geological sea level data are publicly available in published databases and research articles, and are divided here by subregion: (i) the European coastline (García-Artola *et al.* 2018; Meijles *et al.* 2018; Hijma & Cohen 2019), (ii) the British Isles (Shennan *et al.* 2018), (iii) Scandinavia including Svalbard (Tushingham & Peltier 1993; Nordman *et al.* 2015) and (iv) the Russian Arctic (Baranskaya *et al.* 2018). The GNSS data are publicly available from the Nevada Geodetic Laboratory (http://geodesy.unr.edu/). The computed proxy RSL rates are available in table format in the Supporting Information of this paper.

REFERENCES

Ashe, E.L. *et al.*, 2019. Statistical modelling of rates and trends in Holocene relative sea level, *Quat. Sci. Rev.,* **204,** 58–77.

Auriac, A., Whitehouse, P.L., Bentley, M.J., Patton, H., Lloyd, J.M. & Hubbard, A., 2016. Glacial isostatic adjustment associated with the Barents Sea ice sheet: a modelling inter-comparison, *Quat. Sci. Rev.,* **147,** 122–135.

Bamber, J.L., Westaway, R.M., Marzeion, B. & Wouters, B., 2018. The land ice contribution to sea level during the satellite era, *Environ. Res. Lett.,* **13,** doi:10.1088/1748-9326/aac2f0.

Baranskaya, A.V., Khan, N.S., Romanenko, F.A., Roy, K., Peltier, W.R. & Horton, B.P., 2018. A postglacial relative sea-level database for the Russian Arctic coast, *Quat. Sci. Rev.,* **199,** 188–205.

Bell, F.G., Donnelly, L.J., Genske, D.D. & Ojeda, J., 2005. Unusual cases of mining subsidence from Great Britain, Germany and Colombia, *Environ. Geol.,* **47,** 620–631.

Blewitt, G., Kreemer, C., Hammond, W.C. & Gazeaux, J., 2016. MIDAS robust trend estimator for accurate GPS station velocities without step detection, *J. geophys. Res.,* **121,** 2054–2068.

Boillot, G., Dupeuble, P.A. & Malod, J., 1979. Subduction and tectonics on the continental margin off Northern Spain, *Mar. Geol.,* **32,** 53–70.

Bos, M.S., Fernandes, R.M.S., Williams, S.D.P. & Bastos, L., 2013. Fast error analysis of continuous GNSS observations with missing data, *J. Geod.,* **87,** 351–360.

Böse, M., Lüthgens, C., Lee, J.R. & Rose, J., 2012. Quaternary glaciations of northern Europe, *Quat. Sci. Rev.,* **44,** 1–25.

Bradley, S.L., Milne, G.A., Shennan, I. & Edwards, R., 2011. An improved glacial isostatic adjustment model for the British Isles, *J. Quat. Sci.,* **26,** 541–552.

Bridgland, D.R. & Schreve, D.C., 2009. Implications of new Quaternary uplift models for correlation between the Middle and Upper Thames terrace sequences, UK, *Glob. Planet. Change,* **68,** 346–356.

Bungenstock, F. & Weerts, H.J.T., 2010. The high-resolution Holocene sea-level curve for Northwest Germany: global signals, local effects or data-artefacts? *Int. J. Earth Sci.: Geol. Rundsch.,* **99,** 1687–1706.

Carlson, A.E. & Clark, P.U., 2012. Ice sheet sources of sea level rise and freshwater discharge during the last deglaciation, *Rev. Geophys.,* **50,** doi:10.1029/2011RG000371.

Caron, L., Ivins, E.R., Larour, E., Adhikari, S., Nilsson, J. & Blewitt, G., 2018. GIA model statistics for GRACE hydrology, cryosphere, and ocean science, *Geophys. Res. Lett.,* **45,** 2203–2212.

Church, J.A. *et al.* , 2013, Sea level change, in *Climate Change 2013: The Physical Science Basis. Contribution of Working Group I to the Fifth Assessment Report of the Intergovernmental Panel on Climate Change,* pp. 1137–1216, eds, Stocker, T.F. et al., Cambridge Univ. Press.

Cloetingh, S.A.P.L. *et al.*, 2007. Topo-europe: the geoscience of coupled deep earth-surface processes, *Glob. Planet. Change,* **58,** 1–118.

Dangendorf, S., Marcos, M., Wöppelmann, G., Conrad, C.P., Frederikse, T. & Riva, R., 2017. Reassessment of 20th century global mean sea level rise, *Proc. Natl. Acad. Sci. USA,* **114,** 5946–5951.

de Waal, J.A., Muntendam-Bos, A.G. & Roest, J.P.A., 2015. Production induced subsidence and seismicity in the Groningen gas field—can it be managed? *Proc. Int. Assoc. Hydrol. Sci.,* **372,** 129–139.

Delgado, J., Boski, T., Nieto, J.M., Pereira, L., Moura, D., Gomes, A., Sousa, C. & García-Tenorio, R., 2012. Sea-level rise and anthropogenic activities recorded in the late Pleistocene/Holocene sedimentary infill of the Guadiana Estuary (SW Iberia), *Quat. Sci. Rev.,* **33,** 121–141.

Farrell, W.E. & Clark, J.A., 1976. On postglacial sea level, *Geophys. J. R. astr. Soc.,* **46,** 647–667.

Fokker, P.A., van Leijen, F.J., Orlic, B., van der Marel, H. & Hanssen, R.F., 2018. Subsidence in the Dutch Wadden Sea, *Neth. J. Geosci.,* **97,** 129–181.

Frederikse, T., Riva, R., Kleinherenbrink, M., Wada, Y., van den Broeke, M. & Marzeion, B., 2016. Closing the sea level budget on a regional scale: trends and variability on the Northwestern European continental shelf, *Geophys. Res. Lett.,* **43,** 10 864–10 872.

García-Artola, A., Stéphan, P., Cearreta, A., Kopp, R.E., Khan, N.S. & Horton, B.P., 2018. Holocene sea-level database from the Atlantic coast of Europe, *Quat. Sci. Rev.,* **196,** 177–192.

Gowan, E.J., Tregoning, P., Purcell, A., Montillet, J.-P. & McClusky, S., 2016. A model of the western Laurentide Ice Sheet, using observations of glacial isostatic adjustment, *Quat. Sci. Rev.,* **139,** 1–16.

Gregory, J.M. *et al.*, 2019. Concepts and Terminology for sea level: mean, variability and change, both local and global, *Surv. Geophys.,* **40,** 1251–1289.

Hijma, M. & Kooi, H., 2018. Bodemdaling in het kustfundament en de getijdenbekkens (deel 2): Een update, case IJmuiden en kwantificering, Deltares report, 59pp.

Hijma, M.P. & Cohen, K.M., 2019. Holocene sea-level database for the Rhine-Meuse Delta, The Netherlands: implications for the pre-8.2 ka sea-level jump, *Quat. Sci. Rev.,* **214,** 68–86.

Hijma, M.P., Engelhart, S.E., Törnqvist, T.E., Horton, B.P., Hu, P. & Hill, D.F., 2015. A protocol for a geological sea-level database, in *Handbook of Sea-Level Research,* pp. 536–553, eds Shennan, I., Long, A.J. & Horton, B.P., John Wiley & Sons.

Hill, E.M., Davis, J.L., Tamisiea, M.E. & Lidberg, M., 2010. Combination of geodetic observations and models for glacial isostatic adjustment fields in Fennoscandia, *J. geophys. Res.,* **115,** doi:10.1029/2009JB006967.

Holgate, S.J. *et al.*, 2013. New data systems and products at the permanent service for mean sea level, *J. Coast. Res.,* **29,** 493–504.

Hughes, A.L.C., Gyllencreutz, R., Lohne, Ø.S., Mangerud, J. & Svendsen, J.I., 2016. The last Eurasian ice sheets—a chronological database and time-slice reconstruction, DATED-1, *Boreas,* **45,** 1–45.

Humphries, L., 2001. A review of relative sea level rise caused by mining-induced subsidence in the coastal zone: some implications for increased coastal recession, *Clim. Res.,* **18,** 147–156.

Ivins, E.R., James, T.S., Wahr, J., Schrama, E.J.O., Landerer, F.W. & Simon, K.M., 2013. Antarctic contribution to sea level rise observed by GRACE with improved GIA correction, *J. geophys. Res.,* **118,** 3126–3141.

Khan, N.S.the HOLSEA working group *et al.*, and the HOLSEA working group, 2019. Inception of a global atlas of sea levels since the Last Glacial Maximum, *Quat. Sci. Rev.,* **220,** 359–371.

Kiden, P., Denys, L. & Johnston, P., 2002. Late Quaternary sea-level change and isostatic and tectonic land movements along the Belgian–Dutch North Sea coast: geological data and model results, *J. Quat. Sci.,* **17,** 535–546.

Kiden, P., Makaske, B. & van de Plassche, O., 2008. Waarom verschillen de zeespiegelreconstructies voor Nederland, *Grondboor Hamer,* **3/4,** 54–61.

Kierulf, H.P., Steffen, H., Simpson, M.J.R., Lidberg, M., Wu, P. & Wang, H. 2014. A GPS velocity field for Fennoscandia and a consistent comparison to glacial isostatic adjustment models, *J. geophys. Res.,* **119,** 6613–6629.

Klemann, V. & Steffen, H., and the Baltic-SLI team, 2018. A Holocene sea-level database for the Baltic Sea, *Geophys. Res. Abst.,* **20,** EGU2018–5257-2.

Kooi, H., Johnston, P., Lambeck, K., Smither, C. & Molendijk, R., 1998. Geological causes of recent (∼100 yr) vertical land movement in the Netherlands, *Tectonophysics,* **299,** 297–316.

Kuchar, J., Milne, G., Hubbard, A., Patton, H., Bradley, S., Shennan, I. & Edwards, R., 2012. Evaluation of a numerical model of the British–Irish ice sheet using relative sea-level data: implications for the interpretation of trimline observations, *J. Quat. Sci.,* **27,** 597–605.

Lambeck, K., 1997. Sea-level change along the French Atlantic and Channel coasts since the time of the Last Glacial Maximum, *Palaeogeogr. Palaeoclimatol. Palaeoecol.,* **129,** 1–22.

Lambeck, K. & Nakada, M., 1990. Late Pleistocene and Holocene sea-level change along the Australian coast, *Palaeogeogr. Palaeoclimatol. Palaeoecol.,* **89,** 143–176.

Lambeck, K., Purcell, A., Zhao, J. & Svensson, N.-O., 2010. The Scandinavian Ice Sheet: from MIS 4 to the end of the Last Glacial Maximum, *Boreas,* **39,** 410–435.

Lambeck, K., Purcell, A.,Funder, S.,Kjær , K.H.,Larsen, E.& Möller, P.,2006. Constraints on the Late Saalian to early Middle Weichselian ice sheet of Eurasia from field data and rebound modelling, *Boreas,* **35,** 539–575.

Lambeck, K., Smither, C. & Johnston, P., 1998. Sea-level change, glacial rebound and mantle viscosity for northern Europe, *Geophys. J. Int.,* **134,** 102–144.

Leorri, E., Fatela, F., Drago, T., Bradley, S.L., Moreno, J. & Cearreta, A., 2012. Lateglaial and Holocene coastal evolution in the Minho estuary (N Portugal): implications for understanding sea-level changes in Atlantic Iberia, *The Holocene,* **23,** 353–363.

Li, T. & Wu, P., 2019. Laterally heterogeneous lithosphere, asthenosphere and sub-lithospheric properties under Laurentia and Fennoscandia from Glacial Isostatic Adjustment, *Geophys. J. Int.,* **216,** 1633–1647.

Marks, L. *et al.*, 2018. Revised limit of the Saalian ice sheet in central Europe, *Quat. Int.,* **478,** 59–74.

Meijles, E.W., Kiden, P., Streurman, H.-J., van der Plicht, J., Vos, P.C., Gehrels, W.R. & Kopp, R.E., 2018. Holocene relative mean sea-level changes in the Wadden Sea area, northern Netherlands, *J. Quat. Sci.,* **33,** 905–923.

Milne, G.A., Davis, J.L, Mitrovica, J.X., Scherneck, H.-G., Johansson, J.M., Vermeer, M. & Koivula, H., 2001. Space-geodetic constraints on glacial isostatic adjustment in Fennoscandia, *Science,* **291,** 2381–2385.

Mitrovica, J.X. & Milne, G.A., 2003. On post-glacial sea level: I. General theory, *Geophys. J. Int.,* **154,** 253–267.

Morzadec-Kerfourn, M.T., 1995. Coastline Changes in the Armorican Massif (France) During the Holocene, *J. Coast. Res.,* **17,** 197–203.

Noël, B., van de Berg, W.J., van Meijgaard, E., Kuipers Munneke, P., van de Wal, R.S.W. & van den Broeke, M.R., 2015. Evaluation of the updated regional climate model RACMO2.3: summer snowfall impact on the Greenland Ice Sheet, *The Cryosphere,* **9,** 1831–1844.

Nordman, M., Milne, G. & Tarasov, L., 2015. Reappraisal of the Ångerman River decay time estimate and its application to determine uncertainty in Earth viscosity structure, *Geophys. J. Int.,* **201,** 811–822.

Patton, H. *et al.*, 2017. Deglaciation of the Eurasian ice sheet complex, *Quat. Sci. Rev.,* **169,** 148–172.

Patton, H., Hubbard, A., Andreassen, K., Winsborrow, M. & Stroeven, A.P., 2016. The build-up, configuration, and dynamical sensitivity of the Eurasian ice-sheet complex to Late Weichselian climatic and oceanic forcing, *Quat. Sci. Rev.,* **153,** 97–121.

Peltier, W.R., 2004. Global glacial isostasy and the surface of the ice-age Earth: the ICE-5G (VM2) model and GRACE, *Annu. Rev. Earth Planet. Sci.,* **32,** 111–149.

Peltier, W.R. & Andrews, J.T., 1976. Glacial-isostatic adjustment—I. The forward problem, *Geophys. J. R. astr. Soc.,* **46,** 605–646.

Peltier, W.R., Argus, D.F. & Drummond, R., 2015. Space geodesy constrains ice age terminal deglaciation: the global ICE-6G_C (VM5a) model, *J. geophys. Res.,* **119,** doi:10.1002/2014JB011176.

Permanent Service for Mean Sea Level (PSMSL), 2019, ' Tide Gauge Data'. Retrieved 23 Oct 2019 from http://www.psmsl.org/data/obtaining/.

Phillips, E., Hodgson, D.M. & Emery, A.R., 2017. The Quaternary geology of the North Sea basin, *J. Quat. Res.,* **32,** 117–126.

Rietbroek, R., Brunnabend, S.-E., Kusche, J., Schröter, J. & Dahle, C., 2016. Revisiting the contemporary sea-level budget on global and regional scales, *Proc. Natl. Acad. Sci. USA,* **113,** 1504–1509.

Rinterknecht, V. *et al.*, 2018. The last glacial maximum extent of the Scandinavian Ice Sheet in the Valday Heights, Western Russia: evidence from cosmogenic surface exposure dating using ^{10}Be, *Quat. Sci. Rev.,* **200,** 106–113.

Riva, R.E.M. *et al.*, 2009. Glacial isostatic adjustment over Antarctica from combined ICESat and GRACE satellite data, *Earth planet. Sci. Lett.,* **288,** 516–523.

Root, B.C., Tarasov, L. & van der Wal, W., 2015. GRACE gravity observations constrain Weichselian ice thickness in the Barents Sea, *Geophys. Res. Lett.,* **42,** 3313–3320.

Rosentau, A. *et al.*, 2021. A Holocene relative sea-level database for the Baltic Sea, *Quat. Sci. Rev.,* in revision.

Schmidt, P., Lund, B., Näslund, J.-O. & Fastook, J., 2014. Comparing a thermo-mechanical Weichselian Ice Sheet reconstruction to reconstructions based on the sea level equation: aspects of ice configurations and glacial isostatic adjustment, *Solid Earth,* **5,** 371–388.

Sella, G.F., Dixon, T.H. & Mao, A., 2002. REVEL: a model for Recent plate velocities from space geodesy, *J. geophys. Res.,* **107,** ETG 11–1-ETG 11-30.

Shennan, I., 2007. Sea level studies: overview, in *Encyclopedia of Quaternary Science,* pp. 2967–2974, ed. Elias, S.A., Elsevier.

Shennan, I., 2015. Handbook of sea-level research: framing research questions, in *Handbook of Sea-Level Research,* pp. 3–25, eds, Shennan, I., Long, A.J. & Horton, B.P., John Wiley & Sons.

Shennan, I., Bradley, S.L. & Edwards, R., 2018. Relative sea-level changes and crustal movements in Britain and Ireland since the Last Glacial Maximum, *Quat. Sci. Rev.,* **188,** 143–159.

Shennan, I. & Horton, B., 2002. Holocene land- and sea-level changes in Great Britain, *J. Quat. Sci.,* **17,** 511–526.

Shennan, I., Milne, G. & Bradley, S., 2012. Late Holocene vertical land motion and relative sea-level changes: lessons from the British Isles, *J. Quat. Sci.,* **27,** 64–70.

Simon, K.M., James, T.S., Henton, J.A. & Dyke, A.S., 2016. A glacial isostatic adjustment model for the central and northern Laurentide Ice Sheet based on relative sea level and GPS measurements, *Geophys. J. Int.,* **205,** 1618–1636.

Simon, K.M., Riva, R.E.M., Kleinherenbrink, M. & Frederikse, T., 2018. The glacial isostatic adjustment signal at present-day in northern Europe and the British Isles estimated from geodetic observations and geophysical models, *Solid Earth,* **9,** 777–795.

Simon, K.M., Riva, R.E.M.,Kleinherenbrink, M.& Tangdamrongsub, N.,2017. A data-driven model for constraint of present-day glacial isostatic adjustment in North America, *Earth planet. Sci. Lett.,* **474,** 322–333.

Slangen, A.B.A., Katsman, C.A., van de Wal, R.S.W., Vermeersen, L.L.A. & Riva, R.E.M., 2012. Towards regional projections of twenty-first century sea-level change based on IPCC SRES scenarios, *Clim. Dyn.,* **38,** 1191–1209.

Steffen, H. & Wu, P., 2011. Glacial isostatic adjustment in Fennoscandia–a review of data and modeling, *J. Geodyn.,* **52,** 169–204.

Tapley, B.D., Bettadpur, S., Ries, J.C., Thompson, P.F. & Watkins, M.M., 2004. GRACE measurements of mass variability in the Earth System, *Science,* **305,** 503–505.

Tarasov, L., Dyke, A.S., Neal, R.M. & Peltier, W.R., 2012. A data-calibrated distribution of deglacial chronologies for the North American ice complex from glaciological modeling, *Earth planet. Sci. Lett.,* **315–316,** 30–40.

Teferle, F.N. *et al.*, 2009. Crustal motions in Great Britain: evidence from continuous GPS, absolute gravity and Holocene sea level data, *Geophys. J. Int.,* **178,** 23–46.

Thompson, P.R., Hamlington, B.D., Landerer, F.W. & Adhikari, S., 2016. Are long tide gauge records in the wrong place to measure global mean sea level rise, *Geophys. Res. Lett.,* **43,** 10403–10411.

Tushingham, A.M. & Peltier, W.R., 1992. Validation of the ICE-3G Model of Wu¨rm-Wisconsin Deglaciation using a global data base of relative sea level histories, *J. geophys. Res.,* **97,** 3285–3304.

Tushingham, A.M. & Peltier, W.R., 1993. Relative Sea Level Database. IGBP PAGES/World Data Center-A for Paleoclimatology Data Contribution Series # 93-016. NOAA/NGDC Paleoclimatology Program, Boulder CO, USA.

van Casteren, R.A.C.M., 2019. A 3D Glacial Isostatic Adjustment model for Northwestern Europe, *MSc. thesis*, Delft University of Technology, 91pp.

van den Broeke, M.R., Enderlin, E.M., Howat, I.M., Kuipers Munneke, P., Noël, B.P.Y., van de Berg, W.J., van Meijgaard, E. & Wouters, B., 2016. On the recent contribution of the Greenland ice sheet to sea level change, *The Cryosphere,* **10,** 1933–1946.

van der Wal, W., Barnhoorn, A., Stocchi, P., Gradmann, S., Wu, P., Drury, M. & Vermeersen, B., 2013. Glacial isostatic model with composite 3-D Earth rheology for Fennoscandia, *Geophys. J. Int.,* **194,** 61–77.

van Wessem, J.M. *et al.*, 2016. The modelled surface mass balance of the Antarctic Peninsula at 5.5 km horizontal resolution, *The Cryosphere,* **10,** 271–285.

Vermeersen, B.L.A. *et al.*, 2018. Sea-level change in the Dutch Wadden Sea, *Neth. J. Geosci.,* **97,** 79–127.

Vestøl, O., Ågren, J., Steffen, H., Kierulf, H. & Tarasov, L., 2019. NKG2016LU: a new land uplift model for Fennoscandia and the Baltic Region, *J. Geod.,* **93,** 1759–1779.

Vink, A., Steffen, H., Reinhardt, L. & Kaufmann, G., 2007. Holocene relative sea-level change, isostatic subsidence and the radial viscosity structure of the mantle of northwest Europe (Belgium, the Netherlands, Germany, southern North Sea), *Quat. Sci. Rev.,* **26,** 3249–3275.

Walcott, R.I., 1972. Past sea levels, eustasy and deformation of the Earth, *Quat. Res.,* **2,** 1–14.

Westaway, R., 2017. Isostatic compensation of Quaternary vertical crustal motions: coupling between uplift of Britain and subsidence beneath the North Sea, *J. Quat. Sci.,* **32,** 169–182.

Whitehouse, P.L., 2018. Glacial isostatic adjustment modelling: historical perspectives, recent advances, and future directions, *Earth Surf. Dyn.,* **6,** 401–429.

Wouters, B., Bonin, J.A., Chambers, D.P., Riva, R.E.M., Sasgen, I. & Wahr, J., 2014. GRACE, time-varying gravity, Earth system dynamics and climate change, *Rep. Prog. Phys.,* **77,** doi:10.1088/0034-4885/77/11/116801.

Zhao, S., Lambeck, K. & Lidberg, M., 2012. Lithosphere thickness and mantle viscosity inverted from GPS-derived deformation rates in Fennoscandia, *Geophys. J. Int.,* **190,** 278–292.

SUPPORTING INFORMATION

Supplementary data are available at *GJI* online.

Figure S1. RSL data and computed rates for the European Coastline. Grey, sea level index point; red, terrestrial limiting. We have plotted the later Holocene (after 2 kyr BP) data from the Wadden Sea as terrestrial limiting data instead of SLIP data; this modification is suggested to be appropriate by Meijles *et al.* (2018) although the authors did not specifically incorporate this distinction in their data set. Locations/rates which do not meet the criteria to be included in the inversion are labelled as omitted, and indicated in Table S1.

Figure S2. RSL data and computed rates for the British Isles. Locations/rates which do not meet the criteria to be included in the inversion are labelled as omitted, and indicated in Table S1.

Figure S3. RSL data and computed rates for Scandinavia. Locations/rates which do not meet the criteria to be included in the inversion are labelled as omitted, and indicated in Table S1.

Figure S4. RSL data and computed rates for the Russian Arctic. Grey, sea level index point; red, terrestrial limiting; blue, marine limiting. Locations/rates which do not meet the criteria to be included in the inversion are labelled as omitted, and indicated in Table S1.

Figure S5. Predicted vertical land motion and uncertainty values for the G1–G3 models.

Figure S6. Residuals with the VLM data for models G1–G3. $e_{\mathrm{vlm}} = (\mathrm{observed}_{\mathrm{vlm}} - \mathrm{predicted}_{\mathrm{vlm}})$. Small circles indicate absolute values of the residuals that are within data uncertainties, large circles indicate absolute values of the residuals that exceed data uncertainties.

Figure S7. Residuals with the proxy RSL data for models G1–G3. $e_{\mathrm{rsl}} = (\mathrm{observed}_{\mathrm{rsl}} - \mathrm{predicted}_{\mathrm{rsl}})$. Small circles indicate absolute values of the residuals that are within data uncertainties, large circles indicate absolute values of the residuals that exceed data uncertainties.

Table S1. Inferred present-day rates of relative sea level rise for the four regions. 96 curves are considered in total, 71 meet the criteria discussed in the main text for inclusion in the inversion. Highlighted rates are those used in the inversion ($>2\sigma$ significance, or $\sigma \leq 0.5$ mm yr^{-1}, and otherwise not anomalous as discussed below). Rate 1 and σ_1 are inferred from a general least-squares fit, Rate 2 and σ_2 are inferred from an iteratively re-weighted least-squares fit. The latitude and longitude values are in decimal degrees and are the average of the RSL data points used for the rate calculation; individual latitude and longitude values are provided in the original databases. Sources for the original RSL data appear in the second to last columns: European Coastline [García-Artola *et al.* 2018 (G-A2018), Meijles *et al.* 2018 (M2018), Hijma & Cohen 2019 (HC2019)], British Isles [Shennan *et al.* 2018 (S2018)], Scandinavia [Tushingham & Peltier 1993 (TP1993), Nordman *et al.* 2015 (N2015)], Russian Arctic [Baranskaya *et al.* 2018 (B2018)]. Kristiinankaupunki, Finland and the Angermanland, Sweden rates (both from Tushingham & Peltier 1993) and the Timan Coast rate in the Russian Arctic are omitted due to anomalous computed rates. Chupa Bay & the Keret Archipelago, and the Eastern Kola Peninsula, are omitted because they are inferred from terrestrial and marine limiting data only and therefore may not accurately represent the rate of sea level change.

Please note: Oxford University Press is not responsible for the content or functionality of any supporting materials supplied by the authors. Any queries (other than missing material) should be directed to the corresponding author for the paper.